Eur. J. Mineral.
2008, **20**, 857–865
Published online October 2008

This paper is dedicated to the memory of Werner Schreyer

Aragonite–grossular intergrowths in eclogite-facies marble, Alpine Corsica

CHRISTIAN CHOPIN[1,*], OLIVIER BEYSSAC[1], SYLVAIN BERNARD[1] and JACQUES MALAVIEILLE[2]

[1]Laboratoire de Géologie, Ecole normale supérieure – CNRS, 24 rue Lhomond, 75005 Paris, France
*Corresponding author, e-mail: chopin@geologie.ens.fr
[2]Géosciences Montpellier, Université Montpellier 2 – CNRS, Place E. Bataillon, 34095 Montpellier Cedex 5, France

Abstract: The occurrence and preservation of aragonite in eclogite-facies rocks of north-eastern Corsica is linked to an uncommon microtexture. Aragonite exclusively occurs as oriented fibres in garnet crystals of a graphitic, more or less siliceous marble that immediately overlies a serpentinite body of the meta-ophiolitic unit. The arrangement of the fibres is grossly radial, but more clearly sectoral in subhedral garnet, the fibres growing perpendicular to the garnet/matrix interface. Raman mapping reveals that the carbonate is calcite in the matrix and in poikiloblastic garnet cores, and that the fibres in the garnet mantle are aragonite alone in the case of a carbonate matrix, and both aragonite and quartz (in distinct fibres) in a quartz–carbonate matrix. These features are interpreted as prograde intergrowths, the result of garnet nucleation and growth in a calcite and then aragonite matrix (±quartz). Upon further heating and/or decompression, the aragonite matrix transformed back to calcite while the carbonates included in garnet retained their original structure, in spite of the relatively high temperature attained (*ca.* 500 °C). These aragonite relics are one more example of the preservation of a high-pressure polymorph through mechanical shielding of inclusions in a rigid host. The aragonite–garnet intergrowths are similar to quartz–garnet intergrowths described in amphibolite-facies graphitic schists. They are evidence that oriented inclusions in garnet are not necessarily precipitates ('exsolutions'). Unlike precipitates, their orientation is controlled more by the shape of the garnet growth front than by symmetry constraints.

Key-words: aragonite, inclusion, intergrowth, high-pressure relic, blueschist, eclogite facies, garnet, carbonaceous material, Raman mapping, wollastonite, Corsica.

Introduction: the aragonite paradox

Aragonite, a high-pressure $CaCO_3$ polymorph, is expected to form from calcite during incipient subduction of carbonated sediments and, at much higher pressure ($P > 5$ GPa), through the breakdown of dolomite, $CaMg(CO_3)_2$, to $MgCO_3$ (magnesite) + $CaCO_3$ (*e.g.* Martinez *et al.*, 1996; Shirasaka *et al.*, 2002). Aragonite is therefore assumed to be the stable $CaCO_3$ high-pressure form in subducted slabs. However, there are extremely few records of metamorphic aragonite from high-pressure (HP) terranes other than the lowest-temperature, blueschist-facies terranes in which it is classical, like the Franciscan formation in California, or western Crete in Greece.

This paradox has long been recognised as a kinetic issue (Brown *et al.*, 1962; Carlson & Rosenfeld, 1981). The rapid kinetics of the back-transformation of aragonite to calcite make the preservation of metamorphic aragonite to the surface an indicator of decompression under quite low temperatures, implying either anti-clockwise *P–T* paths or at least continuous cooling during decompression. Indeed, records of aragonite relics in high-grade, even eclogite-facies or ultra-high-pressure (UHP) rocks are utterly uncommon. Documented records are 10 μm inclusions (with jadeite and coesite) in zircon from paragneiss in the Dabie UHP terrane (Ye *et al.*, 2002), and nanometre-size inclusions in metamorphic diamond from the Kokchetav massif (Dobrzhinetskaya *et al.*, 2006). In both instances, aragonite could only be identified by high-resolution techniques (Raman microspectroscopy and transmission electron microscopy, respectively), and it occurs as tiny inclusions in a rigid host mineral that prevents expansion and transformation of the high-pressure carbonate into a higher-volume polymorph (in the same way as it does for coesite or microdiamond, *e.g.* Gillet *et al.*, 1984; Sobolev & Shatsky, 1990). Aragonite was also reported both as inclusion in garnet and as a minor matrix phase in eclogite overprinted by blueschist-facies retrograde metamorphism, in an exotic block of the Franciscan Formation (Armstrong *et al.*, 2004; *cf.* Page *et al.*, 2007).

We report here the occurrence and preservation of aragonite in eclogite-facies, hence relatively high-grade metasediments of eastern Corsica. It is one more instance of the mechanical preservation of a high-pressure polymorph within garnet; in addition, the most uncommon microtexture of the aragonite–garnet intergrowths may have an important bearing on the mechanisms of garnet growth and the interpretation of oriented solid inclusions in minerals. We believe that Werner Schreyer, as a keen microscopist, would have appreciated such petrographic *fioretti* and their implications, with his usual enthusiasm in such matters. We take great pleasure and pride in dedicating this preliminary report to the memory of this master, mentor and friend.

0935-1221/08/0020-1892 $ 4.05
DOI: 10.1127/0935-1221/2008/0020-1892
© 2008 E. Schweizerbart'sche Verlagsbuchhandlung, D-70176 Stuttgart

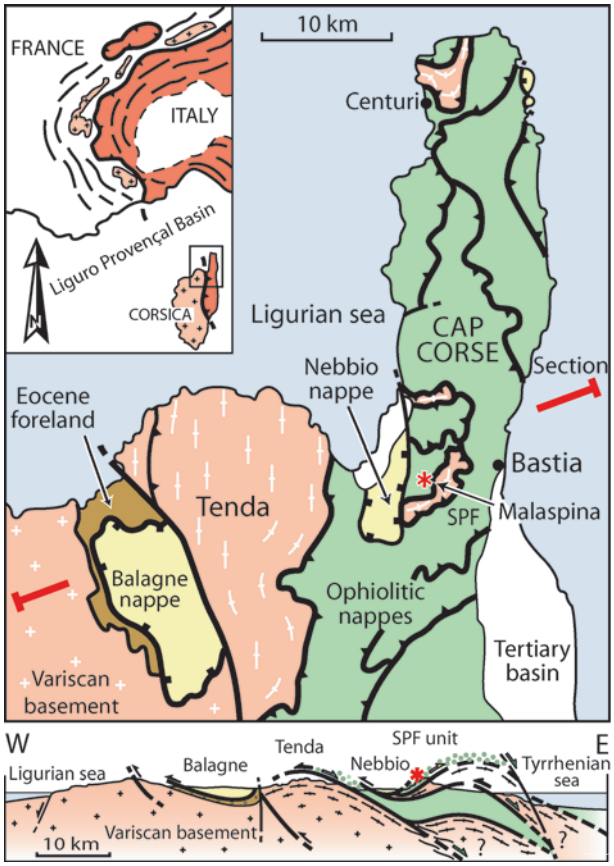

Fig. 1. Geological sketch map and cross-section of the Cap Corse area, NE Corsica, after Malavieille *et al.* (1998). Flesh colour refers to continental units (Variscan basement) with parautochthonous cover (brown), green refers to metamorphic oceanic units, yellow to the uppermost, nearly non-metamorphic nappes. The star indicates the location of the Cima di Malaspina outcrop; SPF = Serra di Pigno/Farinole units. Inset: Alpine chain with internal units (reddish brown) and external crystalline massifs (flesh colour).

Geological setting and occurrence

North-eastern Corsica is part of the Alpine orogen (Fig. 1, inset) and consists mainly of Mesozoic formations of oceanic derivation, some of them possibly transitional between a continental margin (to the west) and more typical ophiolitic units (*e.g.* Faure & Malavieille, 1981; Jolivet *et al.*, 1990; Malavieille *et al.*, 1998, for more details). Most units were metamorphosed during the Alpine orogeny under HP conditions and some reached the lawsonite-eclogite facies, of which they provide a fine, classical example (Caron & Péquignot, 1986; Ravna *et al.*, submitted for publication). In Cap Corse, the northern tip of the island (Fig. 1), the metamorphic pile comprises several ophiolitic units, mostly serpentinite with some gabbro, basalt, peridotite and subordinate sedimentary material including radiolarite and calcschist. Other intercalated units comprise material of more continental derivation, *e.g.* the Farinole/Serra di Pigno gneisses. The Farinole series contain jadeite-bearing metagranite and lawsonite-eclogite, for which early estimates by Lahondère (1988) are $P > 10$ kbar, T(grt–cpx inclusion) ~ 430–520 °C, T(grt–cpx in matrix) ~ 500–600 °C, revised to $P > 15$ kbar, $T \sim 450$–490 °C if one combines Lahondère's (1996) new estimates for orthogneiss and metabasite.[1] More recent estimates for lawsonite-eclogite in meta-pillow-basalts of the Lancône Pass, about 10 km further south, are 24–27 kbar, 450–470 °C (Ravna *et al.*, submitted for publication).

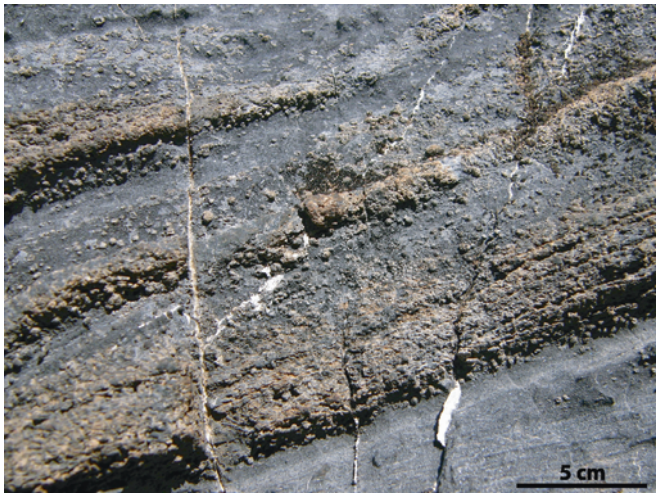

Fig. 2. Outcrop photograph of the garnet-bearing marble layer, within 1 m from the contact to serpentinite. Garnet crystals and the compositional layering are made conspicuous by differential weathering. Cima di Malaspina, Patrimonio, 485 m elevation.

Above the village of Patrimonio, the Malaspina ridge which leads to the Serra di Pigno exposes slivers of a metasedimentary series ranging from marble to carbonate quartzite, in direct contact and refolded with a large serpentinite body (which overlies the Farinole/Serra di Pigno gneisses, which themselves lie structurally above meta-ophiolitic units; Fig. 1). The marble/serpentinite contact is concordant with the sedimentary bedding, as judged from lithological heterogeneities (Fig. 2), and is marked by a continuous, centimetre-thick, weathering-resistant reaction rim of calc-silicates. This sedimentary series may, or may not, represent the stratigraphic cover of a tectonized ocean floor.

Minerals found in the first metres of this series, *i.e.* in the more carbonate-rich layers, are calcite, quartz, garnet, minor diopside, clinozoisite, titanite and apatite, rare albite and abundant graphitic material, locally prehnite. Glaucophane ('crossite') and phengite occur in more pelitic layers. Aragonite was found exclusively in garnet crystals in a black calcite marble layer that immediately overlies the serpentinite, and to which garnet is restricted (Fig. 2). The present report focuses on one such sample and ignores the calc-silicate reaction rim between carbonate series and serpentinite. Noteworthily, yet, wollastonite occurs in this cm-thick calc-silicate rim. It does not occur in our sample nor in the overlying beds. Its identification and local abundance came as a surprise, as this is to our knowledge the first report of wollastonite in high-pressure rocks.

[1] Mineral names abbreviated after Kretz (1983), capitalised for end-members (Aeg for aegirine).

Phase characterization, Raman maps

Beside optical microscopy, electron-microprobe analyses were carried out at Camparis, Université Paris 6 (see Simon & Chopin, 2001, for details of the analytical procedure, except for Sr: $SrSiO_3$ standard, counting 40 s on Sr$L\alpha$ peak). Structural formulae were calculated on the basis of a fixed number of cations to allow a gross estimate of the Fe^{2+}/Fe^{3+} ratio, but on 22 charges for phengite and on a fixed number of tetrahedral cations for epidote-group minerals (Armbruster *et al.*, 2006). Raman microspectroscopy was implemented (i) to characterize the structural state of carbonaceous material in our samples and obtain an estimate of the maximum temperature reached during metamorphism (RSCM, Raman Spectroscopy of Carbonaceous Material thermometry, Beyssac *et al.*, 2002), and (ii) to identify the nature and areal distribution of the $CaCO_3$ polymorphs in thin section, both in point mode and through line-scanning mapping to produce mineral distribution maps.

We used a Renishaw® InVia Raman microspectrometer (at ENS, Paris) equipped with a Modu-Laser Argon Laser (514.5 nm), a 1800 grooves/mm holographic grating and a RENCAM 2d CCD detector. For point analysis, the laser was focussed through a Leica DMLM microscope with a ×100 objective (numerical aperture NA = 0.90) to reach a planar resolution of ~ 1 μm with a laser power delivered at the sample surface of around 1 mW, low enough to avoid laser-induced heating/damaging of the sample.

Raman compositional maps were acquired using the same system with a PRIOR XYZ motorized stage, a ×50 objective (NA = 0.75) and a line focus system which ensures a linear illumination for the laser thanks to a cylindrical lens. We used the Streamline mapping tool recently developed by Renishaw in which the relative mechanical movement of the laser line over the sample is synchronized with the Raman signal acquisition on the CCD detector. This configuration shortens drastically the total acquisition time by up to 50 times compared to point mapping and makes possible the mapping of large areas with high imaging resolution, with sampling step down to 1.1 μm limited by the minimum spot size which is 1 × 1.1 μm (Bernard *et al.*, 2008). Each measured spectrum is subsequently compared to reference spectra, in terms of peak position, width and intensity, using a principal-component analysis method provided by the Renishaw software Wire 3.0. A correlation index 0 to 1 is calculated for each point, with 1 indicating a complete agreement with the reference spectrum. In the maps presented here, a specific colour is assigned to each particular reference mineral spectrum. Each pixel of the mapped area displaying an index value greater than 0.7 for a particular reference (in order to take the signal noise into account) has been represented with the specific colour of this reference.

Petrography

Weathering of the carbonate-rich series reveals a compositional layering due to varying proportions of calcite and quartz in the matrix and, in this matrix, to the varying abundance and size of whitish nodules which turned out to be garnet (Fig. 2). The marble sample studied, about 20 cm across strike, shows the abrupt transition from about 2 cm of pure, very fine-grained (highly strained?) carbonate matrix on the serpentinite side, to a garnet-bearing carbonate matrix in which the proportion of quartz progressively increases away from the contact and in which the size of garnet is first large (several millimetres, Fig. 3A) in a quartz-poor zone (about 1 cm thick) and then rapidly falls to less than 1 mm in the calcite–quartz matrix. Carbonaceous material is ubiquitous, it blurs most grain boundaries but also concentrates into layers that wrap around the garnet porphyroblasts and their pressure shadows. The pure carbonate layer also contains finely dispersed carbonaceous material and thin trails of it. A centimetre-size, coarse-grained polycrystalline diopside boudin occurs in the pure carbonate layer and shows little evidence of rotational deformation. Fine-grained diopside also occurs rather inconspicuously throughout the carbonate–quartz matrix, as a minor component of it.

The largest, millimetre-size garnet crystals concentrated in a 1 cm thick layer of carbonate-rich matrix show an uncommon texture in thin section. They are crowded with more or less radially arranged fibres or rods (Fig. 3A), which are so abundant that the garnet section hardly extinguishes in cross-polarized light (although the garnet itself is *not* birefringent). Closer inspection of subhedral crystals shows that the fibres are actually perpendicular to the faces of the garnet, resulting in a sectoral arrangement of parallel fibres, rather than a radial one (Fig. 3C). The garnets are definitely not of the snowball type. These larger crystals contain hardly any other inclusions than the fibres, which seem to extend from core to rim, and graphite. However, the (nearer to equatorial?) sections of a few crystals show a narrow core zone of poikiloblastic appearance (Fig. 4A, B; Fig. 3B).

The garnet texture changes as the proportion of quartz in the carbonate matrix increases and the garnet size decreases. The fibrous texture in garnet first remains obvious but limited to a thick mantle around a small poikiloblastic core containing a number of equidimensional inclusions (Fig. 4C). Then, in smaller garnet poikiloblasts, fibres become hardly discernible in a thin, massive cloudy rim that bounds a large core zone with honey-comb texture (Fig. 4D). The nearly equidimensional inclusions in the cores are mainly quartz with some carbonate, *i.e.* the matrix components. Their grain size and slight elongation are the same as in the surrounding matrix, implying that little grain coarsening has taken place in the matrix after growth of the core garnet films along grain boundaries. Inclusions of pyroxene were observed both in the core and mantle zones of garnet, mostly as anhedral grains or short prisms, rarely as a few radial fibres in the outer mantle of a garnet in a pyroxene-bearing part of the matrix.

Carbonaceous material imparts a dark colour to the whole rock but, seen in thin section, is not quite evenly distributed. The very fine-grained, pure carbonate zone appears clearer, as well as the carbonate-filled pressure shadows around the large garnets. The garnet crystals themselves, especially the large ones, are also clearer than the average matrix. Actually, carbonaceous material appears as concentrated along the

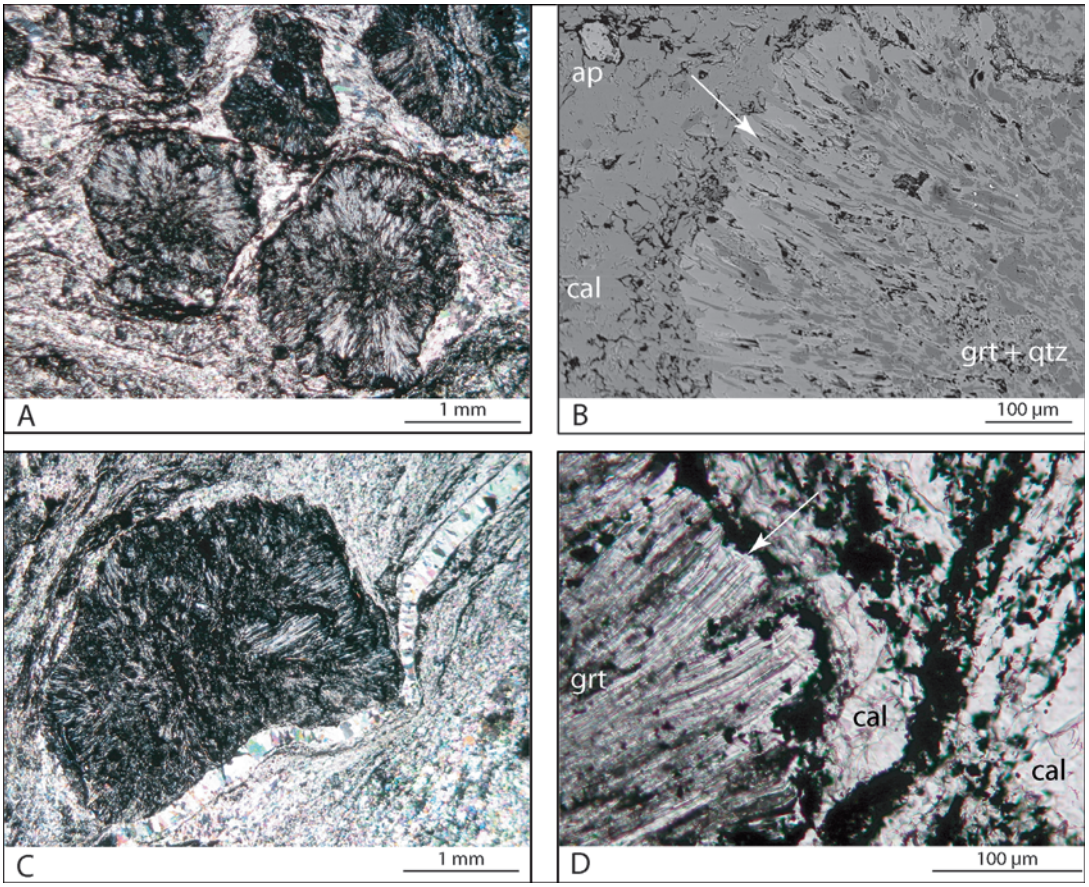

Fig. 3. (A) Photomicrograph of garnet-bearing marble, the zone with the largest garnet crystals in an essentially carbonate groundmass. Note the fibrous appearance of the crystals, the subhedral outline, and the thin selvage of carbonaceous material around them, better seen in D. Cross-polarised light (cpl). (B) Back-scattered electron image of garnet in matrix of carbonate and minor quartz (+apatite, ap). Note the fibres in the garnet mantle, mostly quartz with some aragonite (arrow). (C) Photomicrograph (cpl) of a garnet crystal in the same thin section as A and B, showing that the fibre arrangement is more sectoral (with parallel fibres in a given sector, perpendicular to the crystal face) than strictly radial. Three generations of carbonate are visible: aragonite fibres included in the garnet, fine-grained calcite band (lower right) and matrix (upper left), and late calcite vein. (D) Detailed view (photomicrograph, plane polarized light) of a garnet rim (left-hand side) in a matrix of calcite + carbonaceous matter. Note the selvage of carbonaceous material along the garnet rim, the termination of many fibres in garnet before they reach the rim (arrow), and the crenulated pattern of the garnet/matrix interface, suggesting a much more efficient growth of garnet (and the fibres) perpendicular to the crystal face than laterally. Most fibres are aragonite, a few may be quartz.

margin of these crystals, as if pushed aside during garnet growth (Fig. 3A and D; *cf.* the 'cleavage domes' of Rice & Mitchell, 1991). Some of these packets have been partly engulfed in the garnet margin, imparting it a crenulated outline (Fig. 3D), or simply 'left behind' and entirely incorporated in garnet during its growth (Fig. 3A). In such instances, they commonly interfere with or interrupt the simple fibre pattern. Carbonaceous matter also forms a few nearly ellipsoidal hollow nodules, about 200 µm in size, reminiscent of microfossils. Consistently filled with diopsidic pyroxene (± clinozoisite ± phengite ± quartz), they occur in the matrix but may be included in garnet as well (*e.g.* in the garnet crystal of the central upper part of Fig. 3A).

The fibres in the largest garnet crystals commonly extend from core to rim, as far as can be judged from sections that may not be equatorial. They reach the rim/matrix interface, although there is also some evidence in places of the contrary, *i.e.* of a very narrow outer rim devoid of fibres (Fig. 3D).

Mineralogy and mineral chemistry

Raman spectroscopy (Fig. 4) shows that the fibres are aragonite in the largest garnet crystals (in an essentially calcite matrix), and are both quartz and aragonite in the smaller garnets in the mixed quartz–calcite matrix. In the latter garnets, quartz and aragonite occur as distinct fibres and the proportion of quartz to aragonite fibres increases with increasing quartz content in the matrix (Fig. 4). The anhedral grains included in the poikiloblastic garnet cores are quartz and calcite (Fig. 4). In the sample studied, calcite and aragonite are close to end-member composition (Table 1), with FeO < 0.09 wt.% and MnO < 0.03 wt.%; they are free of Mg except for calcite in the late veins, which bears up to 4 mol% dolomite. The SrO contents are low, typically in the 0.1 wt.% range for both aragonite (up to 0.24 wt.%) and calcite; only late-vein calcite is consistently very low in Sr.

Garnet is grossular, with no evidence of a hydrogarnet component (judging from analytical totals and structural

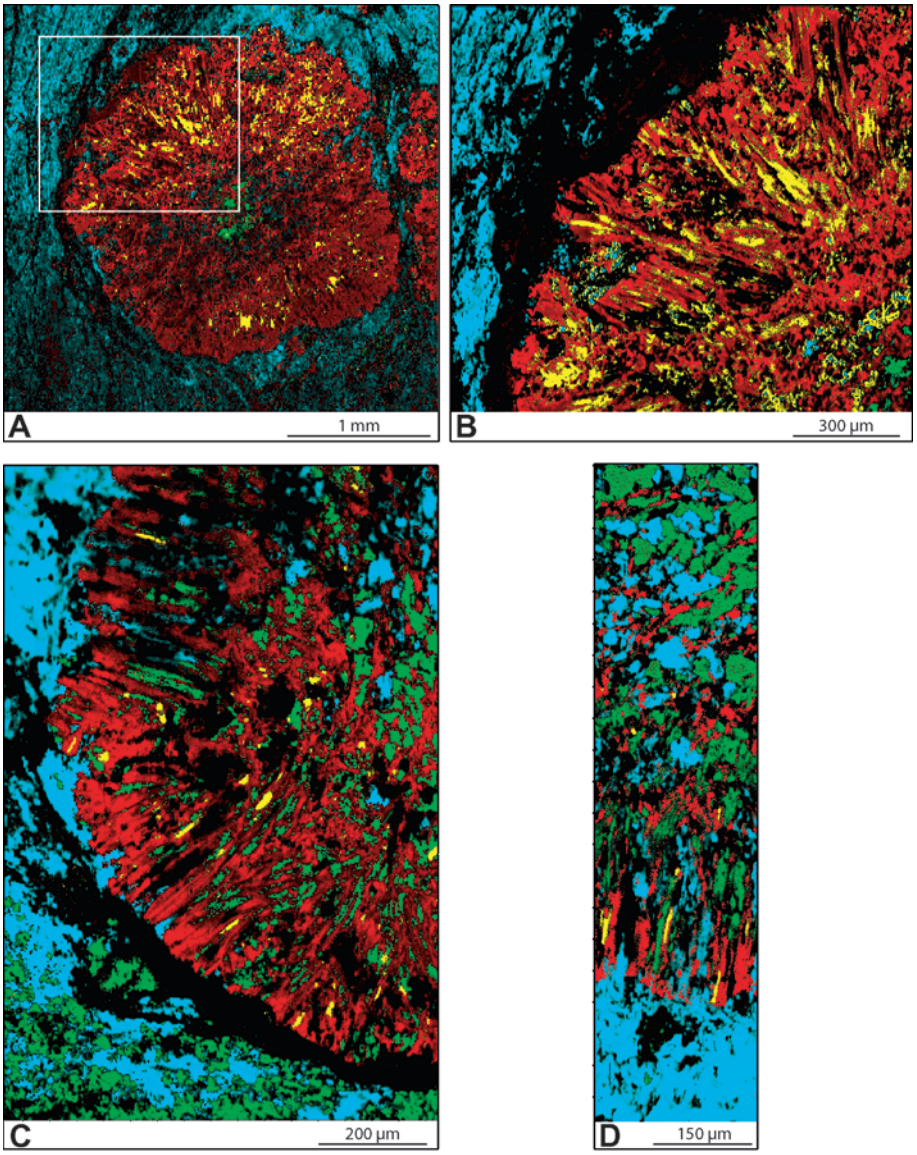

Fig. 4. Raman maps of garnet crystals showing various inclusion patterns and matrix minerals. Colour code: red = garnet, green = quartz, yellow = aragonite, blue = calcite, black is mostly carbonaceous material. (A) Garnet in carbonate-rich matrix; 3010 × 2827 µm, 77 357 spectra, 10 × 11 µm sampling step. Note the calcite matrix, the presence of quartz in the small poikiloblastic core, and of fibrous aragonite in the thick mantle. (B) Enlargement of box in A; 1204.5 × 1356.3 µm, 150 015 spectra, 3.3 × 3.3 µm sampling step. Some aragonite fibres reach the garnet–matrix interface, here against carbonaceous material (upper centre of the picture). Small calcite grains occur locally in garnet (in the large embayment of garnet rim, lower left quarter, and in the inner mantle, lower right corner); their small size and their consistent and intimate association with aragonite suggest that they result from incipient transformation of the latter. (C) Garnet in carbonate–quartz matrix; 807.5 × 1223.2 µm, 179 588 spectra, 2.5 × 2.2 µm sampling step. Note the comparable grain size and shape of quartz and calcite in the matrix and the poikiloblastic garnet core, and the absence there of aragonite associated to calcite, suggesting the primary nature of these calcite inclusions in garnet core (*cf.* A and B). Some aragonite fibres reach the garnet–matrix interface, and the wide fibres of calcite in the garnet rim (upper part of the picture) may be former thick aragonite fibres opening into the matrix and completely back-transformed to calcite. (D) Core to rim section of garnet within carbonate–quartz matrix; 257.4 × 1041.7 µm, 187 506 spectra, 1.3 × 1.1 µm sampling step. In the broad poikiloblastic core zone (upper half of the picture), garnet films interstitial to quartz and calcite are reminiscent of a lace-like or honey-comb texture (*cf.* Hawkins *et al.*, 2007). Thin fibres of quartz and aragonite occur in the more massive garnet rim; one of them reaches the interface with matrix. Broader fibres opening into the matrix and possibly connecting with the core area are calcite and may represent former aragonite fibres.

formulae in Table 1, and from the Raman spectrum in the OH region). It is rather homogeneous near $Grs_{91}Adr_3Alm_4Sps_1$. Compositional variation among crystals is larger than within crystal, but it hardly exceeds ±1 mol% of the Grs, Adr or Alm components. The sole consistent feature in terms of crystal zonation seems to be a slight increase in FeO_{total} and TiO_2 toward the rim (Table 1).

Clinopyroxene is diopside, close to end-member ($Di_{88}Hd_9Jd_2$) in the cm-size, coarse-grained boudin in the carbonate layer; the small grains in the carbonate–quartz

Table 1. Electron-microprobe analyses (wt.%) and structural formulae of minerals in garnet-marble (n.a. = not analysed).

	Garnet			Clinopyroxene			Mica	Epidote	Carbonate		
Site	Core	Mantle	Rim	Boudin	Matrix	Nodule	Nodule	Nodule	Fibre	Matrix	Vein
SiO_2	39.50	39.62	39.38	54.39	52.57	53.81	51.92	38.37			
P_2O_5	0.00	0.05	0.03	0.03	0.03	0.02	0.00	0.06			
Al_2O_3	21.43	21.23	20.41	0.37	2.32	8.79	25.01	30.89			
TiO_2	0.48	0.44	0.57	0.06	0.03	0.10	0.01	0.08			
MgO	0.00	0.05	0.00	16.12	11.84	5.32	3.04	0.03	0.00	0.00	0.71
CaO	34.37	34.64	34.79	24.52	21.97	13.24	0.06	22.69	58.82	58.35	57.31
MnO	0.59	0.41	0.60	0.14	0.27	1.40	0.07	0.02	0.06	0.02	0.00
$FeO_{tot.}$	3.09	2.61	3.26	2.98	7.10	10.50	3.86	3.78	0.09	0.04	0.03
SrO	n.a.	n.a.	n.a.	0.11	0.00	n.a.	0.00	0.29	0.20	0.03	0.03
Na_2O	0.00	0.00	0.03	0.29	1.43	6.73	0.08	0.01			
K_2O	n.a.	n.a.	n.a.	0.03	0.04	n.a.	10.28	0.04			
Total	99.46	99.05	99.07	99.04	97.68	99.91	94.41	96.46	59.17	58.43	58.07
Basis		8 cations			4 cations		11 O	Si + P = 3		1 cation	
Si	3.009	3.027	3.016	2.005	1.992	1.967	3.511	2.996			
P	0.000	0.003	0.002	0.001	0.001	0.001	0.000	0.004			
Al	1.924	1.911	1.843	0.016	0.104	0.379	1.994	2.842			
Ti	0.028	0.025	0.033	0.002	0.001	0.003	0.001	0.005			
Mg	0.000	0.005	0.000	0.886	0.669	0.290	0.306	0.003	0.000	0.000	0.017
Ca	2.805	2.835	2.855	0.969	0.892	0.519	0.004	1.898	0.996	0.999	0.983
Mn	0.038	0.026	0.039	0.004	0.009	0.043	0.004	0.001	0.001	0.000	0.000
Fe	0.197	0.167	0.209	0.092	0.225	0.321	0.218	0.247	0.001	0.001	0.000
Sr				0.002	0.000		0.000	0.013	0.002	0.000	0.000
Na	0.000	0.000	0.005	0.021	0.105	0.477	0.010	0.001			
K				0.001	0.002		0.887	0.003			

matrix are more Na and Fe-rich, near $Di_{67}Hd_{22}Jd_{10}$. In some of the ellipsoidal nodules of carbonaceous material, pyroxene may be even more jadeite-rich, reaching omphacite composition (to $Jd_{38}Aeg_{10}Di_{29}Hd_{22}$) and bearing Fe^{3+}, consistent with the presence there of clinozoisite (Table 1). In such a nodule, the sole phengite flake found has 3.51 Si pfu (Table 1). Apatite is Cl-free, with F < 2.3 wt.%; titanite contains less than 2.2 wt.% Al_2O_3 and 0.2 wt.% FeO_{tot}.

Carbonaceous matter is similar to polycrystalline graphite. Raman microspectroscopy showed some variability in its structural state, with no relation to the textural position (whether included in garnet, or located along garnet rims or within the matrix). The spectra obtained correspond to a maximum metamorphic temperature of 495 °C, with a range (uncertainty) of less than ±15 °C and a calibration-attached accuracy of ±50 °C (Beyssac *et al.*, 2002), a very conservative estimate (*cf.* Beyssac *et al.*, 2004).

Discussion

Metamorphic conditions, aragonite preservation

The maximum temperature attained is well constrained near 500 °C by Raman microspectrometry. Pressure is more difficult to evaluate if one restricts the observations to the outcrop or to the lithological unit considered. Strictly, the *P–T* estimates obtained on characteristic lawsonite eclogite and jadeite–garnet–glaucophane–chloritoid–paragonite assemblages (20.5 ± 1.2 kbar and 485 ± 15 °C, Lahondère *et al.*, in preparation) apply to units that are underlying the present one. However, considering that our ongoing survey with RSCM thermometry shows temperatures around 470–500 °C in the lawsonite-eclogite-facies units of Cap Corse, and around 380 °C in the overlying units in which Mg–Fe–carpholite relics are preserved and no eclogite occurs, we assign the Malaspina section to the same lawsonite-eclogite facies as underlying units, on the basis of the high temperature obtained.

The presence of aragonite at such high temperature is puzzling, but cannot be taken at face value to derive a minimum pressure (about 11 kbar at 500 °C according to the aragonite–calcite equilibrium curve, *e.g.* Hacker *et al.*, 2005). Indeed, the exclusive presence of aragonite as inclusion in a rigid host-mineral like garnet mechanically prevents its back transformation to a lower-pressure, higher-volume polymorph, even in a temperature range where transformation kinetics are rapid (*cf.* Gillet *et al.*, 1984; Van der Molen & Van Roermund, 1986; Sobolev *et al.*, 2000). In other words, this maximum temperature may have been reached outside the aragonite stability field, even if aragonite is preserved.

Besides, the relatively high peak-temperature derived is in line with the occurrence of wollastonite in the inner part of the calc-silicate reaction zone between the carbonate series and serpentinite at Malaspina. Wollastonite implies very low XCO_2 in the fluid phase attending its formation (XCO_2 < 0.0004 at 490 °C and 10 kbar, according to the database of Berman (1988) including the equation of state and mixing properties of H_2O–CO_2 by Kerrick & Jacobs, 1981). However, such conditions must have been restricted to the contact zone with serpentinite, because quartz +$CaCO_3$ remained stable throughout the rest of the profile, including our sample.

The presence of titanite rather than rutile with quartz + carbonate in the profile sets an upper bound for X_{CO_2} (< 0.02 at 500 °C, 10 kbar; < 0.12 at 500 °C, 5 kbar); the presence of grossular rather than clinozoisite + quartz + calcite in our sample narrows the conditions to $X_{CO_2} < 0.004$ at 500 °C, 10 kbar; < 0.01 at 500 °C, 5 kbar).

Aragonite significance: a growth scenario

The presence of calcite (+quartz, Fig. 4C, D) in the poikiloblastic garnet cores is a key point; it shows that garnet nucleation took place in a calcite–quartz matrix, before the growth of the rim containing aragonite + quartz fibres. This is evidence that aragonite cannot be a metastable relic from the sedimentary stage – a question that may arise since the presence of aragonite in/on serpentinite ocean-floor is well documented (*e.g.* Ribeiro *et al.*, 2008).

Besides, a secondary origin for the aragonite fibres within garnet is not conceivable either; the hypothesis of a carbonate precipitate ('exsolution') within a garnet matrix is chemically untenable if one considers the volume ratio of carbonate fibres and host silicate, and it would have a crystallographic control reflecting all the symmetry operators of the host-mineral, which is not the case (at any given place in garnet, one single fibre direction is observed).

The origin of the fibres must therefore be primary. Their shape and orientation and the crystallographic continuity of each fibre imply that the fibres cannot have pre-existed in a rock matrix but that they have been trapped during garnet growth. Clearly, they must have nucleated and grown during garnet growth, by some competitive growth process of the two phases, leading to the present texture which is best characterised as a *prograde intergrowth*.

The most likely scenario is therefore the following. Whether or not aragonite was present in the sediment, garnet nucleated along the prograde path in a quartz–calcite ± diopside matrix and started to grow in a poikiloblastic way, trapping nearly isometric quartz, calcite and rare diopside inclusions. At some later stage, the calcite-aragonite transition was sufficiently overstepped for the reaction to proceed, transforming the matrix into an aragonite ± quartz groundmass. Garnet growth continued in the quartz–carbonate matrix and started in the carbonate matrix (to the extent that the garnet crystals there do not show poikiloblastic cores but aragonite fibres from core to rim), in both instances with fibrous rather than isometric inclusions. Calcite inclusions in the poikiloblastic cores did not convert to aragonite, as they were mechanically shielded by the rigid host garnet (*e.g.* Gillet *et al.*, 1984; Van der Molen & Van Roermund, 1986). Later, upon decompression or/and heating out of the aragonite stability field, the aragonite matrix transformed back to calcite while the carbonates included in garnet retained their original structure (calcite in poikiloblastic cores and aragonite in the fibres) thanks again to mechanical shielding by the rigid host.

The back-transformation of the matrix must have occurred above about 250 °C for kinetic reasons (*e.g.* Sotin & Madon, 1988); it most likely took place after cessation of garnet growth, because the garnet does not seem to contain calcite inclusions in its outer rim. In this respect, the manner in which the aragonite fibres merge out of the garnet rim and whether they show some degree of transformation into calcite when they are in open connection with the matrix is of particular relevance. However, the common accumulation of carbonaceous matter along garnet rims makes observation and a definite answer difficult. In some instances, the aragonite ± quartz fibres clearly 'neck down' within the garnet rim without reaching the matrix (Fig. 3D) but this may not be the general case. Fibres in many garnet crystals do reach the interface with the matrix (especially with the carbonaceous material, Fig. 4B, C) and the Raman maps suggest that calcite may penetrate a few tens of μm, replacing some of the broadest aragonite fibres. Nowhere is the impression given of a prograde trapping of calcite inclusion in garnet rims.

The whole metamorphic history may be relatively simple and the preservation of aragonite in such a high-grade, garnet-bearing rock is solely due to the mechanical shielding of fibrous inclusions. That such preservation has not been more often recognized may be due to the fact that minute carbonate inclusions are seldom checked for their exact nature. Indeed, tiny aragonite blebs have just been discovered within coesite inclusions in garnet from Erzgebirge eclogite (O'Brien & Ziemann, 2008, this issue), as a by-product of Raman mapping dedicated to the coesite inclusions. In our case, the conspicuous texture was the incentive for a closer investigation. The origin of this uncommon texture remains a main point of discussion.

Origin of the intergrowths

How and why did these intergrowths form? Why did garnet growth in the carbonate–quartz matrix change from poikiloblastic to a competitive one with aragonite fibres? An interesting feature is that the most euhedral garnet crystals show that the fibre growth is not strictly radial but rather tends to be sectoral, with the fibres oriented perpendicular to the growing free face bounding the sector toward the matrix (Fig. 3C). This feature is very reminiscent of the spectacular inclusion pattern of quartz fibres described by Andersen (1984) in almandine–kyanite–staurolite schist from amphibolite-facies rocks of North Cape, Norway. The similarity in size, spacing and aspect ratio of the fibres, in their arrangement perpendicular to the growing surface, is striking (Fig. 2 and 3 in Andersen, 1984). These features of sectoral growth with oriented quartz fibres were also observed in other garnets (*cf.* Fig. 100A in Harker, 1939) and elegantly rationalized by Burton (1986, his Fig. 1) as a coeval growth of quartz fibres parallel to the [110] direction of garnet, *i.e.* perpendicular to the growing face in each of the twelve symmetry-equivalent pyramids making up rhombododecahedral garnet. In these cases, the additional trapping of tiny isometric grains of matrix minerals (mostly graphite and ilmenite) by the lateral growth of adjacent faces results in typical inclusions trails along sector boundaries (type-1 inclusions of Andersen, 1984 – the very inclusion pattern typical for 'chiastolite' andalusite and 'trapiche' emerald).

A relevant point made by Burton (1986) is that the quartz–garnet intergrowths are confined to graphite-bearing layers, with a sharp contrast in garnet zonation and inclusion pattern across the boundary between graphite-free and graphite-bearing layer (his Fig. 4). This led him to the hypothesis that the composition of the attending fluid (X_{CH_4}, X_{CO_2}, *etc.*), in reducing the solubility of quartz, may determine the appearance of such intergrowths. Indeed, the growth of the fibres along with that of the garnet face implies dissolution in the matrix and reprecipitation at the growing face, with a necessary component redistribution between fibre tips and garnet face. Implicit in this hypothesis is that, the lower the solubility, the more a local process (nucleation and precipitation) is favoured (over migration and precipitation). The 'graphite' rim around garnet may be the insoluble residue left as evidence of matrix dissolution. Through its shielding effect, it isolates the garnet face from the abundant quartz or carbonate nuclei present in the matrix and so can make quartz or carbonate nucleation at the garnet surface (and then growth of regularly spaced fibres) energetically more favourable than overgrowth on preexisting seeds in the matrix.

The Corsican occurrence confirms the relation to beds rich in carbonaceous material; however, it also shows that this intergrowth pattern in garnet is not restricted to quartz but simply involves the main matrix mineral(s): it may be quartz alone in pelitic schist (Norway), but aragonite in a carbonate matrix (Fig. 3A, C; Fig. 4A, B), or aragonite + quartz in a carbonate + quartz matrix (Fig. 3B, 4C, D) and may also involve diopside in pyroxene-bearing parts of the matrix. If one considers unlikely that phases as different as quartz, pyroxene and carbonate may show a same dependence of their solubility on fluid composition, the chemical effect of graphite through fluid composition as proposed by Burton (1986) may not be determining. More effective would be the screening effect of the graphite layer progressively accumulating on the garnet face, insulating the growing face from the nuclei present in the matrix (after an initial stage during which garnet growth is still poikiloblastic). One may also think of a change in the wetting properties of the fluid, or of other surface effects of graphite, like site poisoning. It may or may not be relevant that the few instances of the rare fibrous habit developed by mica or chlorite are in very graphite-rich systems (Raith & Vali, 1998).

However, graphite may not be the ultimate explanation. Indeed, graphite-free pyrometamorphic rocks of the Hatrurim Formation in Israel, which may have reached 900 °C or more during oil or gas combustion, provide another spectacular example of such intergrowths (Sokol *et al.*, 2008; Gross, 1977): rods of nagelschmidtite, $(Ca,K)_2(Si,P)O_4$, are sectorally arranged in schorlomite garnet (also in melilite) in a groundmass of wollastonite, rankinite, kalsilite, *etc.* The 'tubular inclusions' show an extremely regular shape and distribution in garnet. These features bear some kinship with *cellular precipitation* reactions in alloys (*cf.* Hacker *et al.*, 2005, about rods of magnesian calcite in aragonite) and *symplectite* formation (Ashworth & Chambers, 2000), even if in the latter two cases a pre-existing phase (alloy, or olivine for instance) provides locally the components of the intergrowth. In our case, the grossular-forming reaction is unclear but, on textural grounds, it is unlikely that garnet replaced a pre-existing phase like lawsonite, prehnite or (clino)zoisite, and mass transport may have played a role. In any event, the principle underlying the solid-state formation of intergrowths with grains elongated perpendicular to the reaction front from which the product minerals grow, is the difficult diffusion of some components as compared to growth rate, and the balance between diffusive energy dissipation and grain-boundary energy (*e.g.* Ashworth & Chambers, 2000).

At this preliminary stage of investigation, the factor that governed this balance and the change in garnet growth from poikiloblastic to fibrous in our sample is still unclear, as it was for the change from honeycomb to massive in the high-pressure garnets studied in much greater detail by Hawkins *et al.* (2007).

Implications: prograde intergrowths *vs.* 'exsolutions'

In spite of this uncertainty, the recognition of these oriented rods or fibres as a primary growth feature, rather than a secondary precipitate, has some general bearing. Oriented inclusions, in particular in garnet, must not necessarily be secondary precipitates ('exsolutions'), as commonly assumed in recent literature. Considering the far-reaching implications that actual precipitates may have in terms of high pressure or temperature of formation of the parent mineral (*e.g.* Liu *et al.*, 2007), it is essential to establish sound discrimination criteria between primary growth features and secondary precipitates. The crystallographic control on a precipitate must be a strong one, revealing the symmetry of the host; for the fibrous intergrowths, a single direction is expressed locally within the crystal, it is perpendicular to the growing interface and so coincides with a crystallographic direction only when the growing surface is an actual crystal face. Otherwise, even a bending of the fibres is possible, reflecting changes in the shape of the growing interface, and should be characteristic of an intergrowth.

Last, we hope this report will be received as a call for a new look at oriented inclusions in minerals – for which Raman mapping can be a powerful tool.

Acknowledgements: The senior author is most indebted to Torgeir Andersen, Oslo, for the loan of his Magerøy specimen, to Ella Sokol, Novosibirsk, for sharing her enthusiasm for the Hatrurim Formation, to Bernard Evans for supporting advice, to Hans-Joachim Massonne and Lutz Nasdala for constructive and timely reviews, and to the guest editors of this issue for their long patience. Funding by INSU DyETI and ANR JC GeoCarbons to OB is acknowledged.

References

Andersen, T.B. (1984): Inclusion patterns in zoned garnets from Magerøy, north Norway. *Mineral. Mag.*, **48**, 21-26.

Armbruster, T., Bonazzi, P., Akasaka, M., Bermanec, V., Chopin, C., Gieré, R., Heuss-Assbichler, S., Liebscher, A., Menchetti, S., Pan, Y., Pasero, M. (2006): Recommended nomenclature of epidote-group minerals. *Eur. J. Mineral.*, **18**, 561-567.

Armstrong, L.S., Page, F.Z., Essene, E.J. (2004): Two generations of sphene in one garnet from a Franciscan eclogite, Healdsburg, California. *Geol. Soc. Am. Abstr. Progr.*, **36**, 135.

Ashworth, J.R. & Chambers, A.D. (2000): Symplectic reaction in olivine and the controls of intergrowth spacing in symplectite. *J. Petrol.*, **41**, 285-304.

Berman, R.G. (1988): Internally-consistent thermodynamic data for stoichiometric minerals in the system Na_2O–K_2O–CaO–MgO–FeO–Fe_2O_3–Al_2O_3–SiO_2–TiO_2–H_2O–CO_2. *J. Petrol.*, **29**, 445-522.

Bernard, S., Beyssac, O., Benzerara, K., Belleil, M., Evans, G.A. (2008): Raman mapping using advanced line-scanning systems: geological applications. *Appl. Spectrosc.*

Beyssac, O., Goffé, B., Chopin, C., Rouzaud, J.-N. (2002): Raman spectra of carbonaceous material in metasediments: a new geothermometer. *J. Metamorphic Geol.*, **20**, 859-871.

Beyssac, O., Bollinger, L., Avouac, J.P., Goffé, B. (2004): Thermal metamorphism in the Lesser Himalaya of Nepal determined from Raman spectroscopy of carbonaceous material. *Earth Planet. Sci. Lett.*, **225**, 233-241.

Brown, W.H., Fyfe, W.S., Turner, F.J. (1962): Aragonite in California glaucophane schists, and the kinetics of the aragonite-calcite transition. *J. Petrol.*, **3**, 566-587.

Burton, K.W. (1986): Garnet–quartz intergrowths in graphitic pelites: the role of the fluid phase. *Mineral. Mag.*, **50**, 611-620.

Carlson, W.D. & Rosenfeld, J.L. (1981): Optical determination of topotactic aragonite–calcite growth-kinetics – metamorphic implications. *J. Geol.*, **89**, 615-638.

Caron, J.-M. & Péquignot, G. (1986): The transition between blueschists and lawsonite-bearing eclogites based on observations from Corsican basalts. *Lithos*, **19**, 205-218.

Dobrzhinetskaya, L.F., Wirth, R., Green II, H.W. (2006): Nanometric inclusions of carbonates in Kokchetav diamonds from Kazakhstan: a new constraint for the depth of metamorphic diamond crystallization. *Earth Planet. Sci. Lett.*, **343**, 85-93.

Faure, M. & Malavieille, J. (1981): Etude structurale d'un cisaillement ductile: le charriage ophiolitique corse dans la région de Bastia. *Bull. Soc. Géol. France*, **23**, 335-342.

Gillet, Ph., Ingrin, J., Chopin, C. (1984): Coesite in subducted continental crust: *P–T* history deduced from an elastic model. *Earth Planet. Sci. Lett.*, **70**, 426-436.

Gross, S. (1977): The Mineralogy of the Hatrurim Formation, Israel. *Geol. Surv. Isr. Bull.*, **70**.

Hacker, B.R., Rubie, D.C., Kirby, S.H., Bohlen, S.R. (2005): The calcite–aragonite transformation in low-Mg marbles: equilibrium relations, transformation mechanisms, and rates. *J. geophys. Res.*, **110** B03205, doi: 10.1029/2004JB003302.

Harker, A. (1939): Metamorphism. Methuen, London.

Hawkins, A.T., Selverstone, J., Brearley, A.J., Beane, R.J., Ketcham, R.A., Carlson, W.D. (2007): Origin and mechanical significance of honeycomb garnet in high-pressure metasedimentary rocks from the Tauern Window, Eastern Alps. *J. Metamorphic Geol.*, **25**, 565-583.

Jolivet, L., Dubois, R., Fournier, M., Goffé, B., Michard, A., Jourdan, C. (1990): Ductile extension in Alpine Corsica. *Geology*, **18**, 1007-1010.

Kerrick, D.M. & Jacobs, G.K. (1981): A modified Redlich-Kwong equation for H_2O, CO_2, and H_2O–CO_2 mixtures at elevated pressures and temperatures. *Am. J. Sci.*, **281**, 735-767.

Kretz, R. (1983): Symbols for rock-forming minerals. *Am. Mineral.*, **68**, 277-279.

Lahondère, D. (1988): Le métamorphisme éclogitique dans les orthogneiss et les métabasites ophiolitiques de la région de Farinole (Corse). *Bull. Soc. Géol. France*, **4**, 579-585.

— (1996): Les schistes bleus et les éclogites à lawsonite des unités continentales et océaniques de la Corse alpine. *Doc. B.R.G.M.*, **240**, 286 p.

Liu, L., Zhang, J.F., Green, H.W., Jin, Z.N., Bozhilov, K.N. (2007): Evidence of former stishovite in metamorphosed sediments, implying subduction to > 350 km. *Earth Planet. Sci. Lett.*, **263**, 180-191.

Malavieille, J., Chemenda, A., Larroque, C. (1998): Evolutionary model for Alpine Corsica: mechanism for ophiolites emplacement and exhumation of high-pressure rocks. *Terra Nova*, **10**, 317-322.

Martinez, I., Zhang, J., Reeder, R.J. (1996): In situ X-ray diffraction of aragonite and dolomite at high pressure and high temperature: evidence for dolomite breakdown to aragonite and magnesite. *Am. Mineral.*, **81**, 611-624.

O'Brien, P.J. & Ziemann, M.A. (2008): Preservation of coesite in exhumed eclogite: insights from Raman mapping. *Eur. J. Mineral.*, **20**, DOI: 10.1127/0935-1221/2008/0020-1883.

Page, F.Z., Armstrong, L.S., Essene, E.J., Mukasa, S.B. (2007): Prograde and retrograde history of the Junction School eclogite, California, and an evaluation of garnet–phengite–clinopyroxene thermobarometry. *Contrib. Mineral. Petrol.*, **153**, 533-555.

Raith, J.G. & Vali, H. (1998): Fibrous chlorite and muscovite from the Kaisersberg graphite mine, Styria Austria. *Can. Mineral.*, **36**, 741-754.

Ravna, E.K., Krogh Ravna, E.J., Andersen, T.B., Jolivet, L. (Submitted for publication): New insights into the formation of lawsonite eclogites – constraints from prograde evolution of eclogitized pillow lava from Corsica. *Contrib. Mineral. Petrol.*

Ribeiro da Costa, I., Barriga, F.J.A.S., Taylor, R.N. (2008): Late seafloor carbonate precipitation in serpentinites from the Rainbow and Saldanha sites (mid-Atlantic Ridge). *Eur. J. Mineral.*, **20**, 173-181.

Rice, A.H.N. & Mitchell, J.I. (1991): Porphyroblast textural sector-zoning and matrix displacement. *Mineral. Mag.*, **55**, 379-396.

Shirasaka, M., Takahashi, E., Nishihara, Yu., Matsukage, K., Kikegawa, T. (2002): In situ X-ray observation of the reaction dolomite = aragonite + magnesite at 900–1300 K. *Am. Mineral.*, **87**, 922-930.

Simon, G. & Chopin, C. (2001): Enstatite–sapphirine crack-related assemblages in ultrahigh-pressure pyrope megablasts, Dora-Maira massif, western Alps. *Contrib. Mineral. Petrol.*, **140**, 422-440.

Sobolev, N.V. & Shatsky, V.S. (1990): Diamond inclusions in garnet from metamorphic rocks: a new environment for diamond formation. *Nature*, **343**, 742-746.

Sobolev, N.V., Fursenko, B.A., Goryainov, S.V., Shu, J.F., Hemley, R.J., Mao, H.K., Boyd, F.R. (2000): Fossilized high pressure from the Earth's deep interior: the coesite-in-diamond barometer. *Proc. Natl. Acad. Sci. USA*, **97**, 11875-11879.

Sokol, E.V., Novikov, I.S., Zateeva, S.N., Sharygin, V.V., Vapnik, Ye. (2008): Pyrometamorphic rocks of the spurrite–merwinite facies as indicators of hydrocarbon discharge zones (the Hatrurim Formation, Israel). *Doklady Earth Sciences*, **420**, 608-614.

Sotin, C. & Madon, M. (1988): Generalized nonlinear inversion of kinetics data: application to the calcite = aragonite transformation. *Phys. Earth Planet. Int.*, **52**, 159-171.

Van der Molen, I. & Van Roermund, H.L.M. (1986): The pressure path of solid inclusions in minerals: the retention of coesite inclusions during uplift. *Lithos*, **19**, 317-324.

Ye, K., Liu, J.B., Cong, B.L. (2002): Ultrahigh-pressure (UHP) low-Al titanites from carbonate-bearing rocks in Dabieshan-Sulu UHP terrane, eastern China. *Am. Mineral.*, **87**, 875-881.

Received 10 July 2008
Modified version received 30 July 2008
Accepted 1 August 2008